Analysis and Design of Bio-Inspired Circuits with Locally-Active Memristors

Alon Ascoli, *Senior Member, IEEE*, Ahmet Samil Demirkol, Ronald Tetzlaff, *Senior Member, IEEE*, and Leon Chua, *Life Fellow, IEEE*

***Abstract*—As established by the second law of thermodynamics, an isolated system is unable to exhibit complex behaviours. Conversely, a physical system, which interacts with the surrounding environment, may support emergent phenomena, provided some of its constitutive components are capable to amplify infinitesimal fluctuations in energy under suitable polarization, a property which is referred to as Local Activity. Local Activity is in fact a New Universal Physics Principle, which, grounded on solid theoretical foundations, enables to explain emergent phenomena in any open system, e.g. the generation of All-or-None electrical spikes in neurons, and Symmetry-Breaking Effects in biological homogeneous cellular media. The existence of solid-state memristor nano-devices, which, similarly as the sodium and potassium ion channels, may operate in the Local Activity domain under opportune bias conditions, opens up new opportunities to synthesise circuits and systems, which, operating according to biological principles, may outperform traditional computing structures in terms of time and energy efficiency. This tutorial aims to shed light on the precious role that Nonlinear Circuit and System Theory shall assume in the years to come to support the exploration of the full potential of memristor physical realizations, which clearly show signs of Local Activity while admitting a Negative Differential Resistance upon suitable DC excitation, for bio-inspired electronics.**

***Index Terms*— Local Activity, Edge of Chaos, Complexity, Volatile Memristors, Negative Differential Resistance, Bio-Inspired Circuit Design, Hopf and Fold Limit Cycle Bifurcations**

I. INTRODUCTION

WITH CMOS scaling approaching atomic boundaries [1], both industry and academia are devoting tremendous efforts in exploring the potential of disruptive nanotechnologies, enabling the realization of multi-purpose devices, which may allow to extend the functionalities or resolve the issues of traditional computing machines, so as to foster progress in integrated circuit design beyond the Moore era [2]. In this regard, memristor devices [3], capable to combine data sensing, storage and processing functionalities within a single miniaturized physical volume, may open up a large number of new opportunities in the world of electronics ([4], [5], [6]). The fabrication of dense crossbar arrays of memristor physical realisations from the non-volatile class across the metal layers of a standard CMOS manufacturing process allows to reserve the third dimension of the overall hardware architecture to execute memory tasks, with a concurrent reduction in the area of the underlying transistor-based circuitry [7]. Moreover, exploiting the dynamical law, governing the time evolution of the state of each of its memristive elements under stimulation, crossbar arrays can also be employed as data processing engines, e.g. to accelerate vector-matrix multiplications [8] or to perform Boolean logic operations [9], allowing the implementation of time- and energy-efficient in-memory computing paradigms ([10], [11], [12]). However, this is just one side of the story. Volatile resistance switching memories, featuring a Negative Differential Resistance branch on the DC current versus voltage characteristic ([13], [14], [15], [16]), are expected to assume a pivotal role for the synthesis of brain-like computing machines in the years to come. In fact, similarly as the ion channels [17] in the axon membrane of a biological neuron [18], these memristors may act as Small-Signal Amplifiers upon suitable polarization, a property which qualifies them as Locally Active devices, and enables the hardware implementation of spike-based computing paradigms [19] to boost the performance of traditional electronic circuits, besides paving the way toward the realization of biologically-plausible neuromorphic networks [20]-[21] to improve our understanding of the operating principles of living systems. A robust and systematic design of a bio-inspired electrical network with Locally Active memristors requires the application of Circuit- and System-Theoretic techniques [22]-[23], including, most importantly, methods from the Physics Principle of Local Activity [24] and from Nonlinear Dynamics Theory [25], in order to draw a preliminary comprehensive picture of its local and global behaviors. Being aware of all the factors, playing a critical role in these dynamics, the designer would then be in the favourable position to choose an optimal set for the parameters so as to ensure the circuit would feature pre-defined functionalities even in case non-ideal effects would perturb it away from the nominal operating conditions, which may arise, for example, due to the inherent variability of memristor devices. Complementing the theory with an insightful pedagogical example, regarding the design of an oscillator, exploiting the Negative Differential Resistance (NDR) of a niobium oxide (NbO_x) memristor from NaMLab

This manuscript was received on September 10, 2023, revised on December 1, 2023, and accepted on December 2, 2023. The research of L. Chua was supported in part by the U.S. Air Force Office of Scientific Research (AFOSR) under Grant FA 9550-18-1-0016. A. Ascoli is with the Department of Electronics and Telecommunications, Politecnico di Torino, Turin, Italy. A.S. Demirkol, and R. Tetzlaff are with the Faculty of Electrical and Computer Engineering, Technische Universität Dresden, Dresden, Germany. L. Chua is with the Department of Electrical Engineering and Computer Sciences, University of California, Berkeley, Berkeley, CA, United States. The corresponding author is A. Ascoli (e-mail: alon.ascoli@polito.it).

[26], this tutorial provides a good overview of the theoretical methods necessary to synthesize robust bio-inspired circuits and systems, which, leveraging the rich dynamics of Locally Active memristors, process data similarly as biological cells [27], and networks ([28], [29]) do.

II. Local Activity and Edge of Chaos Theory

A two-terminal dynamical circuit element, endowed with n states, and driven by some signal u, in voltage (current) form, is Locally Active about an operating point[1] $\boldsymbol{Q} = (X_1, \dots, X_n)$, where it is preliminarily polarized by a DC input[2] U, if and only if there exists an infinitesimal stimulus δu, which, added up to the bias level U from a certain time instant t_0, induces a small-signal response δy, in current (voltage) form, from the device, such that the net local energy $\delta\mathcal{E}(t, t_0)$, the device itself absorbs over the time frame $[t_0, t]$, with $t > t_0$, i.e.

$$\delta\mathcal{E}(t; t_0) = \int_{t_0}^{t} \delta u(t') \cdot \delta y(t') dt', \tag{1}$$

goes negative[3] for at least one finite time instant $t = \bar{t}$. Despite its rigor, this definition is impractical for testing purposes. However, such investigation may be facilitated if the one-port admits a DC output Y-input U characteristic, according to the guidelines, established by the *Local Activity Theorem* [30], asserting that a n^{th}-order two-terminal circuit element is Locally Active at a certain operating point $\boldsymbol{Q}$ if and only if at least one of the following four conditions holds true:

1) The i^{th} pole $s = p_i$ of the local transfer function[4] $H(s; \boldsymbol{Q}) = (\mathcal{L}\{\delta y(t)\}/\mathcal{L}\{\delta u(t)\})|_{\boldsymbol{Q}}$, evaluated at $\boldsymbol{Q}$, is located on the *Right Half of the Complex Plane (RHP), $i \in \{1,2 \dots, n\}$.*

2) A single pole $p_i = j\omega_i$ of the local transfer function $H(s; \boldsymbol{Q})$, evaluated at $\boldsymbol{Q}$, lies along the $j\omega$ axis, and the associated residue[5] is either a complex number or a negative real number, $i \in \{1,2 \dots, n\}$.

3) Each of m poles of the local transfer function $H(s; \boldsymbol{Q})$, evaluated at $\boldsymbol{Q}$, from the set $\{p_k, p_{k+1}, \dots, p_{k+m-1}\}$, with $k \in \{1, \dots, n-m+1\}$, $m \leq n$, and $m \in \{2, \dots, n-k+1\}$, appears at the same position along the $j\omega$ axis.

4) The real part of the local frequency response $\Re\{H(j\omega; \boldsymbol{Q})\}$, evaluated at $\boldsymbol{Q}$, goes negative at some finite real-valued angular frequency ω_0.

The *Edge of Chaos Corollary* [30] establishes that a n^{th}-order two-terminal circuit element is poised on the Edge of Chaos at some operating point $\boldsymbol{Q}$ if and only if it is locally-active and asymptotically stable at $\boldsymbol{Q}$. This occurs on the proviso that the two conditions to follow concurrently hold true:

1) All the n poles of the local transfer function $H(s; \boldsymbol{Q})$, evaluated at $\boldsymbol{Q}$, sit on the Left Half of the Complex Plane (LHP).

2) The real part of the local frequency response $\Re\{H(j\omega; \boldsymbol{Q})\}$, evaluated at $\boldsymbol{Q}$, goes negative at some real angular frequency $\omega_0 \in (-\infty, +\infty)$.

III. Exploring Local Activity and Edge of Chaos in Memristors

Featuring a DC output-input characteristic is a necessary yet insufficient requirement for a memristive one-port to act as a small-signal amplifier under suitable polarization. As a result, non-volatile memristor physical realizations, for which a DC characteristic cannot be defined, are unable to display a Locally Active behaviour. Conversely, a volatile memristor typically exhibits a DC characteristic. In order to test a device of this kind for Local Activity at one of its operating points, its local transfer function should be preliminarily derived.

A. Memristor Model and DC Response Investigation

In order to study the DC response of a volatile memristor, the availability of a predictive model is of critical importance. The one-port, under the zooming lens in the pedagogical circuit design example to follow, is a NbOx threshold switch, known as NaMLab memristor [23], which belongs to the class of volatile Locally Active resistance switching memories, analogously as the vanadium oxide device [31]. Invoking the Unfolding Theorem [32], a large data set, experimentally acquired via static and dynamic measurements from device samples, was employed to derive polynomial series expansions for the state evolution function $g(x, v)$ and memductance $G(x)$ of a first-order voltage-controlled generic memristor model, reading as

$$\dot{x} = g(x, v) \triangleq a_0 + a_1 \cdot x + b_2 \cdot v^2 + c_{21} \cdot v^2 \cdot x + c_{22} \cdot v^2 \cdot x^2 + c_{23} \cdot v^2 \cdot x^3 + + c_{24} \cdot v^2 \cdot x^4 + c_{25} \cdot v^2 \cdot x^5, \text{ and} \tag{2a}$$

$$i = \hat{\imath}(x, v) \triangleq G(x) \cdot v = (d_0 + d_1 \cdot x + d_2 \cdot x^2 + d_3 \cdot x^3 + d_4 \cdot x^4) \cdot v, \tag{2b}$$

where i, v, and x stand for the device current, voltage and state, respectively. The values of the parameters in this differential algebraic equation (DAE) set are given in Table I.

TABLE I
Parameter setting for the DAE set (2a)-(2b), as fitted to a NbOx passive yet locally-active memristor [26]

a_0	a_1	b_2	c_{21}
$5.19 \cdot 10^9$	$-2.05 \cdot 10^7$	$7.21 \cdot 10^9$	$-0.07 \cdot 10^9$
c_{22}	c_{23}	c_{24}	c_{25}
$+2.27 \cdot 10^5$	$-2.4 \cdot 10^2$	$1.25 \cdot 10^{-1}$	$-2.69 \cdot 10^{-5}$
d_0	d_1	d_2	d_3
$6.50 \cdot 10^{-3}$	$-6.66 \cdot 10^{-5}$	$2.14 \cdot 10^{-7}$	$-2.14 \cdot 10^{-10}$
d_4			
$1.19 \cdot 10^{-13}$			

As experimentally revealed in preliminary experiments, under current sweep the entire DC characteristic of the NbOx device is observable (see Fig. 1(a)). This is not the case, when the

[1] The i^{th} state of the two-terminal dynamical circuit element is denoted as x_i, while its bias value is indicated as X_i, for each i value from the set $\{1,2, \dots, n\}$. Also, in general, the bias value of an electrical variable is indicated by capitalizing the associated symbol.

[2] The response of the one-port to the DC stimulus U is indicated as Y.

[3] The net energy $\mathcal{E}(t; t_0)$, which is absorbed by a Globally Passive voltage (current)-controlled one-port, such as the NaMLab memristor, from t_0 to t, and may be computed as the time integral of the instantaneous power $u \cdot y$, where $u = \delta u + U$ and $y = \delta y + Y$ stand respectively for the overall device voltage (current) input and for the overall device current (voltage) output, over the time interval $[t_0, t]$, may never go negative.

[4] Assuming an input variable in voltage (current) form, i.e. $u = v$ ($u = i$), implying an output variable in current (voltage) form, i.e. $y = i$ ($y = v$), the local transfer function $H(s; \boldsymbol{Q})$ of the voltage (current)-controlled one-port about some operating point $\boldsymbol{Q}$ corresponds in fact to its small-signal admittance $Y(s; \boldsymbol{Q}) = (\mathcal{L}\{\delta i(t)\}/\mathcal{L}\{\delta v(t)\})|_{\boldsymbol{Q}}$ (small-signal impedance $Z(s; \boldsymbol{Q}) = (\mathcal{L}\{\delta v(t)\}/\mathcal{L}\{\delta i(t)\})|_{\boldsymbol{Q}}$) at $\boldsymbol{Q}$.

[5] The residue is computed via $r_{p_i} = \lim_{s \to p_i} (s - p_i) \cdot H(s; \boldsymbol{Q})$.

locus is acquired under voltage stimulation. Here, as shown in Fig. 1(b), only the branches, featuring a positive slope, along which the device admits a positive differential resistance, PDR for short, are visible. The remaining branches are unstable. Since their negative slope endows the device with a negative differential resistance (NDR), which is a signature for Local Activity, as elucidated shortly, understanding the origin for this instability is the next step of the investigation. The Dynamic Route Map (DRM) technique [33] is instrumental to clarify this point. The generic memristor model, expressed in (2a)-(2b), may be recast in current-controlled form as

$$\dot{x} = g(x, R(x)\cdot i), \text{ and} \quad (3a)$$
$$v = \hat{v}(x,i) = R(x)\cdot i, \text{ with } R(x) = G^{-1}(x). \quad (3b)$$

Plotting the state evolution function from (3a) versus the state for a given DC current $i = I$, and superimposing arrows[6], pointing to the east (west) on the upper (lower) half of the $\dot{x}$ versus x plane, along the resulting locus, provides a State Dynamic Route (SDR) [34] for the NaMLab memristor under current control. As shown in Fig. 2(a), illustrating the family of SDRs, i.e. the DRM, of the ordinary differential equation (ODE) (3a), each directed trace crosses the horizontal axis with negative slope[7] only in one point, whose abscissa constitutes the globally asymptotically stable (GAS) operating point[8] $Q \triangleq X$ of the NaMLab memristor for the associated DC current I. This explains why the whole DC V versus I locus is stable (refer to Fig. 1(a)). Referring now to the voltage-controlled case, plotting the state evolution function from (2a) against the state, the resulting locus intersects the horizontal axis with negative slope in a single point, whose abscissa represents a GAS operating point for the device, if and only if the DC voltage V, let fall across the one-port, falls within either of the PDR ranges. However, if V is chosen from a NDR range, the $\dot{x}$ versus x locus admits three crossings with the horizontal axis (see Fig. 2(b)). As may be inferred by inspecting the direction of the arrows along a locus of this kind, the abscissa of each of the outer ones, corresponds to a locally-stable PDR bias point. The abscissa of the inner one is however associated to an unstable NDR operating point. Clearly, this is the reason why the NDR branches of the I versus V characteristic are unstable (consult Fig. 1(b)). A simple circuit design strategy allows to stabilize a NDR bias point $P = (V, I)$ of the device under voltage control. With reference to Fig. 3(a), the strategy envisages the insertion of a linear and passive resistor R_S between a DC voltage source V_S and the NaMLab memristor, indicated through the symbol $\mathcal{M}$. With reference to Fig. 4(a), the bias parameter pair (V_S, R_S) need to be chosen in such a way that the DC load line $I = (V_S - V)/R_S$ meets the DC current versus voltage locus of the device in the NDR bias point only. This ensures that the SDR of the ODE (2a), where $v = \tilde{v}(x, V_S) = V_S/(1 + G(x)\cdot R_S)$, crosses with negative slope the state axis in a single point,

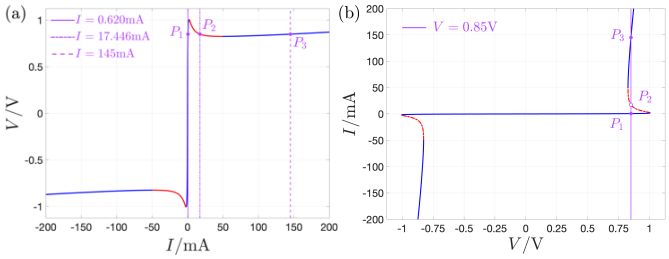

Fig. 1 (a) ((b)) DC characteristic of the NaMLab memristor under current (voltage) sweep. In the first case, any given DC load line $i = I$ crosses the DC V versus I characteristic only once, identifying a single admissible bias point $P = (I, V)$ for the device. as is the case for each I value from the set $\{0.620, 17.446, 145\}$mA. In the latter case, the DC load line $v = V$ may cross the DC I versus V characteristic as many as three times, identifying three possible bias points $P_1 = (V, I_1)$, $P_2 = (V, I_2)$, and $P_3 = (V, I_3)$ for the device, when the bias voltage falls within a NDR range, as is the case for $V = 0.85$V, when $I_1 = 0.620$mA, $I_2 = 17.446$mA, and $I_3 = 145$mA. A red (blue) color is used to mark NDR (PDR) branches in either DC locus. A solid (dash-dotted) line style is adopted to highlight branches of stable (unstable) bias points in (a) and (b). The bias point, at which the solid, dash-dotted, and dashed violet load line in (a) crosses the DC V versus I locus corresponds to the first, second, and third point of intersection between the violet load line and the DC I versus V locus in (b). With reference to the first quadrant of either characteristic, which appears to be symmetric about the origin, the lower and upper PDR ranges for the device DC current I (DC voltage V) are [0A, 2.036mA), and (49.297mA, 500mA], ([0V, 1.007V) and (0.826V, 1.046V]) respectively. Correspondingly, [253, 351) and (1006, 1722] are the lower and upper PDR ranges for the device operating point Q, respectively.

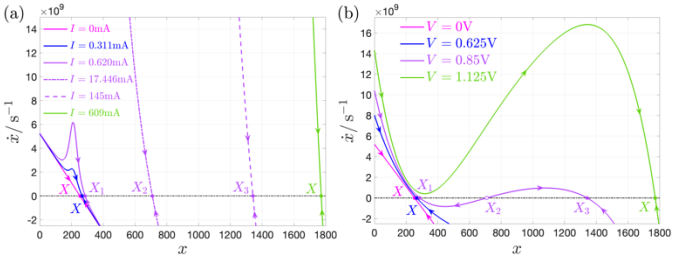

Fig. 2 (a) ((b)) DRM of the NaMLab memristor under current (voltage) sweep. In the first case each DC current endows the memristor with a GAS operating point $Q = X$. In the latter case, if the DC voltage is chosen from a NDR range, e.g. for $V = 0.85$V, the device admits two locally-stable PDR operating points $Q_1 = X_1$ and $Q_3 = X_3$ besides one unstable NDR one $Q_2 = X_2$. Each pair of SDRs, sharing the magenta, blue, or green color in (a) and (b) admit the same crossing with the horizontal axis. The only intersection between the horizontal line and each of the violet SDRs, featuring a solid, dash-dotted, or dashed line style in (a), corresponds respectively to the first, second, and third zero crossing of the violet SDR in (b) (recall also the discussion on the load lines, shown in plots (a) and (b) of Fig. 1, as reported in the respective caption). As a final remark, note that the DRM of the NaMLab device under voltage (current) control from plot (a) ((b)) in this figure is independent of the sign of V (I). Of course, under $I < 0$A ($V < 0$V) the load line in Fig. 1(a) (1(b)) would stretch along the second and fourth quadrants. The NDR range for the operating point Q of the NaMLab memristor is defined as $(Q_{NDR,L}, Q_{NDR,U})$, with $Q_{NDR,L} = 351$ and $Q_{NDR,U} = 1006$.

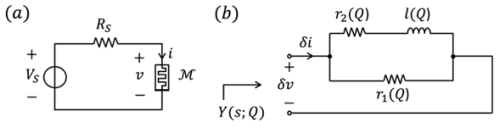

Fig. 3 (a) Bias circuit for stabilizing a NDR bias point of the NaMLab memristor under voltage control. (b) Device local equivalent circuit model.

[6] In the upper (lower) half of the $\dot{x}$ versus x plane, where $\dot{x}$ is positive (negative), x is bound to increase (decrease) over time, which explains the west-to-east (east-to-west) direction of the arrows along the state evolution function versus state locus under a given DC input.

[7] An operating point Q for the one-port under a given DC stimulus is asymptotically stable (unstable), if and only if $(\partial\dot{x}/\partial x)|_Q$ is found to be negative (positive). In the first (latter) case the crossing between the relevant SDR and the horizontal axis is indicated as a filled (hollow) circle.

[8] While the operating point of the current-controlled device is indicated as $Q = X$, the corresponding bias point is referred to as $P = (I, V)$. Q is referred to as a PDR (NDR) operating point if, correspondingly, P lies along a PDR (NDR) branch of the DC V versus I characteristic. Similar conventions are employed *mutatis mutandis* in the voltage-controlled case.

corresponding to a GAS operating point $Q = X$, and unequivocally associated to the bias point of interest (see Fig. 4(b)).

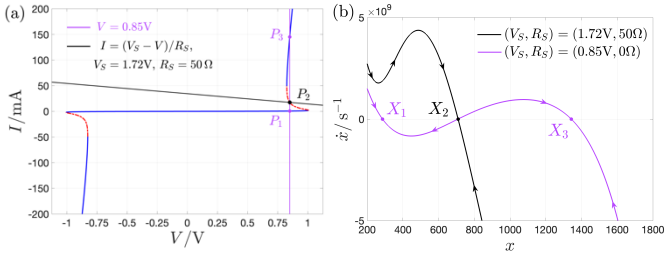

Fig. 4 Illustration of the circuit design strategy for the stabilization of a NDR bias point of the device under voltage control, namely $P = (V, I)$, with $V = 0.85$V, and $I = 17.446$mA. (a) Graphical determination of the admissible bias points for the device, loading a V_S-R_S series one-port (see Fig. 3(a)), as crossings between its DC I versus V locus and the load line for each (V_S, R_S) pair in the set $\{(0.85\text{V}, 0\Omega), (1.72\text{V}, 50\Omega)\}$. (b) SDRs of the NaMLab memristor, which, together with the resistor and the voltage source, forms the three-element circuit of Fig. 3(a), for each of the two aforegiven bias parameter pairs. The NDR operating point $Q = X = 709$ is stabilized only for $(V_S, R_S) = (1.72\text{V}, 50\Omega)$. The filled circle in (a) ((b)) refers to the stable device bias (operating) point for such bias parameter setting. In this case R_S is larger than the modulus of the inverse of the slope of the DC I versus V locus.

B. Testing the Memristor for Local Activity and Edge of Chaos

Without loss of generality, let us consider the voltage-controlled form (2a)-(2b) of the device model. A DC voltage V is preliminarily applied across the device. Let us assume that, consequently, the device state (current) asymptotically converges to some DC value X (I). An infinitesimally-small voltage stimulus δv is then superimposed on top of the bias level V. Let δx (δi) denote the device small-signal state (current) response. The formulas for the device overall voltage, current, and state are then $v = V + \delta v$, $x = X + \delta x$, and $i = I + \delta i$, respectively. Linearizing (2a) and (2b) about a generic operating point $Q = X$ gives

$$\frac{d\delta x}{dt} = a(Q) \cdot \delta x + b(Q) \cdot \delta v, \text{ and} \quad (4a)$$

$$\delta i = c(Q) \cdot \delta x + d(Q) \cdot \delta v, \quad (4b)$$

with $a(Q) \triangleq (\partial g(x,v)/\partial x)|_Q$, $b(Q) \triangleq (\partial g(x,v)/\partial v)|_Q$, $c(Q) \triangleq (\partial \hat{\imath}(x,v)/\partial x)|_Q$, and $d(Q) \triangleq \partial(\hat{\imath}(x,v)/\partial v)|_Q$. Mapping the small-signal model (4a)-(4b) into the Laplace domain, simple algebraic manipulations enable to derive the formula for the device small-signal admittance $Y(s)$. When evaluated at Q, it reads as

$$Y(s;Q) = \frac{\mathcal{L}\{\delta v(t)\}}{\mathcal{L}\{\delta i(t)\}}\Big|_Q = K_Y(Q) \cdot \frac{s - z_Y(Q)}{s - p_Y(Q)}, \quad (5)$$

where $K_Y(Q) = d(Q)$, $z_Y(Q) = (a(Q) \cdot d(Q) - b(Q) \cdot c(Q))/d(Q)$, and $p_Y(Q) = a$. Importantly, the electrical system of Fig. 3(b), known as memristor small-signal equivalent circuit model, features the same admittance as reported in (5), provided its three circuit elements depend upon Q according to $r_1(Q) = 1/d(Q)$, $r_2(Q) = -a(Q)/b(Q) \cdot c(Q)$, and $l(Q) = 1/(b(Q) \cdot c(Q))$. While r_1 and l are strictly positive, r_2 goes negative in the NDR region. Importantly, as the frequency of the small-signal voltage stimulus tends to zero, the device local admittance reduces to $Y(0;Q) \equiv g(Q) = r_1^{-1}(Q) + r_2^{-1}(Q)$, which denotes its small-signal conductance, corresponding to the slope of the DC I versus V characteristic. As g is negative throughout the NDR branch of this locus, condition 4) of the Local Activity Theorem holds true for $\omega = 0$ at any of NDR operating point Q. This explains why NDR effects in a memristive one-port are a signature for Local Activity.

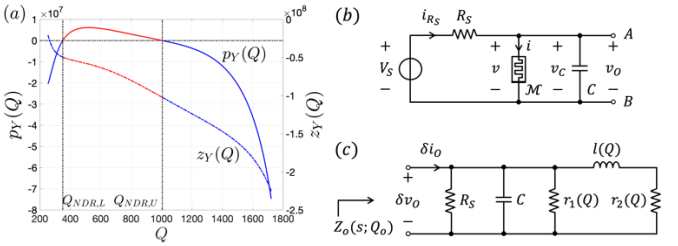

Fig. 5 (a) Loci of p_Y (solid trace) and z_Y (dash-dotted trace) versus Q. A blue (red) color is employed to highlight either PDR range (the NDR range) of the device operating point Q. (b) Second-order bio-inspired cell. (c) Local model of the circuit in (b).

Letting the frequency of the local voltage stimulus tend to infinity, the formula for $Y(s;Q)$ boils down to $r_1^{-1}(Q) \equiv G(Q)$, which denotes the value of the memductance at the operating point. This is expected from a generic memristor, which acts as a linear resistor under very-high frequency excitation. Fig. 5(a) depicts the pole-zero diagram of the device local admittance. While the zero z_Y is strictly negative, the pole p_Y turns positive at each operating point Q in the range $(Q_{NDR,L}, Q_{NDR,U})$, where $Q_{NDR,L} = 351$, and $Q_{NDR,U} = 1006$. This[9] confirms the results drawn via DRM analysis in section III.A: under current (voltage) control, all the (only the PDR) operating points of the NaMLab memristor are stable. Moreover, it is easy to verify that the real part of the device local admittance, evaluated for $s = j\omega$, goes negative[10] across an angular frequency range $\Delta\omega(Q)$, including all frequencies satisfying the inequality $|\omega(Q)| < 1/(-l(Q) \cdot r_2(Q) \cdot (r_1(Q) + r_2(Q)))$, provided the radicand is non-negative, which is the case if and only if Q is a NDR operating point, since the sum between r_1 and r_2 is found to be strictly positive. Thus, for either voltage or current control signal form, the NaMLab memristor is Locally Passive at any PDR operating point. Under voltage (current) control, the device is Locally Active yet Unstable (Locally Active and Stable, i.e. on the Edge of Chaos) at any NDR operating point.

IV. Bio-inspired Oscillator Design

A. Cell Model

An autonomous circuit must be endowed with at least two degrees of freedom to act as an oscillator. Placing a capacitor C in parallel to the memristor $\mathcal{M}$ in the circuit of Fig. 3(a), the resulting second-order cell (see Fig. 5(b)), is described by

$$\dot{x} = f_1(x,v) \triangleq g(x,v), \text{ and} \quad (6a)$$

$$\dot{v} = f_2(x,v) \triangleq \frac{1}{C} \cdot \left(\frac{V_S - v}{R} - \hat{\imath}(x,v)\right), \quad (6b)$$

where x and v stand for memristor state and capacitor voltage, which embody one degree of freedom each, while $g(x,v)$ and $\hat{\imath}(x,v)$ are defined in (2a) and (2b), respectively. Let us denote

[9] The local impedance $Z(s)$ of a one-port is the inverse of its local admittance $Y(s)$. Using (5), the local impedance of the NaMLab device reads as $Z(s) = K_Z \cdot (s - z_Z)/(s - p_Z)$, with $K_Z = K_Y^{-1}$, $z_Z = p_Y$, and $p_Z = z_Y$.

[10] Condition 4) of the Local Activity Theorem may be applied indifferently to each of these local transfer functions. Either choice delivers the same result.

a generic operating point for the cell as $\boldsymbol{Q_O} \triangleq (Q = X, V)$.

B. Testing the Cell for Local Activity and Edge of Chaos

It is worthy[11] to derive the local input impedance $Z_o(s)$ of the respective circuit across the capacitor port A-B. Fig. 5(c) depicts the small-signal equivalent circuit model of the cell of Fig. 5(b) about a given operating point $\boldsymbol{Q_O}$. It was easily derived from Fig. 5(b) by switching off the DC voltage source, and replacing the memristor with its small-signal equivalent circuit model of Fig. 3(b). Analysing the circuit of Fig. 5(c), the small-signal input impedance $Z_o(s;\boldsymbol{Q_o})$ of the cell of Fig. 5(b) across the capacitor port A-B about $\boldsymbol{Q_o}$ is found to read as

$$Z_o(s;\boldsymbol{Q_o}) = K_{Z_o} \cdot \frac{s - z_{Z_o}(\boldsymbol{Q_o})}{\left(s - p_{-,Z_o}(\boldsymbol{Q_o})\right)\cdot\left(s - p_{+,Z_o}(\boldsymbol{Q_o})\right)}, \quad (7)$$

where $K_{Z_o} = 1/C$, $z_{Z_o}(\boldsymbol{Q_o}) = -r_2(Q)/l(Q)$, $p_{\mp,Z_o}(\boldsymbol{Q_o}) = (\tau_{Z_O}(\boldsymbol{Q_O}) \mp \eta_{Z_O}^{1/2}(\boldsymbol{Q_O}))/2$, $\eta_{Z_O}(\boldsymbol{Q_O}) = \tau_{Z_O}^2(\boldsymbol{Q_O}) - 4\cdot\Delta_{Z_O}(\boldsymbol{Q_O})$, $\tau_{Z_O}(\boldsymbol{Q_O}) = -r_2(Q)/l(Q) - 1/(C\cdot(r_1(Q) \parallel R_S))$, and $\Delta_{Z_O}(\boldsymbol{Q_O}) = (1 + r_2(Q)/(r_1(Q) \parallel R_S))/(l(Q)\cdot C)$. For the stability of the cell operating point $\boldsymbol{Q_O}$, it is necessary for $\tau_{Z_O}(\boldsymbol{Q_O})$ and $\Delta_{Z_O}(\boldsymbol{Q_O})$ to be negative and positive, respectively. Now, $\tau_{Z_O}(\boldsymbol{Q_O}) > 0$ if and only if $Q \in (Q_{NDR,L}, Q_{NDR,U})$, and $C > \hat{C}(X)$, where

$$\hat{C}(X) \triangleq -\frac{l(Q)}{r_2(Q)\cdot(r_1(Q) \parallel R_S)}, \quad (8)$$

Moreover, $\Delta_{Z_O}(\boldsymbol{Q_O}) < 0$ if and only if $Q \in (Q_{NDR,L}, Q_{NDR,U})$, and[12] $R_S < -r(Q)$. Last but not least, the real part of $Z_o(j\omega;\boldsymbol{Q_o})$ is found to be negative across the range $\Delta\omega(\boldsymbol{Q_o})$ of frequencies, which satisfy the inequality $|\omega(\boldsymbol{Q_o})| < (-r_2(Q)\cdot(r_2(Q) + r_1(Q) \parallel R_S)/l^2(Q))^{1/2}$, as long as $Q \in (Q_{NDR,L}, Q_{NDR,U})$, and $R_S > -r(Q)$. We may thus conclude that the cell is Locally Passive at $\boldsymbol{Q_o}$ if $Q \notin (Q_{NDR,L}, Q_{NDR,U})$. Moreover, it is Locally Active yet Unstable if $Q \in (Q_{NDR,L}, Q_{NDR,U})$, when either $R_S < -r(Q)$ applies, or both $R_S > -r(Q)$, and $C > \hat{C}(X)$ hold true. Finally, it is poised on the Edge of Chaos at $\boldsymbol{Q_o}$ if $Q \in (Q_{NDR,L}, Q_{NDR,U})$, $R_S > -r(Q)$, and $C < \hat{C}(X)$. The insights, drawn by recurring to the powerful concepts of the Local Activity Theory, shed light into the impact of each design parameter on the local dynamics of the cell. In fact, if[13] the bias parameter pair (V_S, R_S) is chosen so that the DC load line crosses the I versus V locus in one PDR bias point Q for the memristor only, the cell is found to admit a Locally Passive GAS operating point $\boldsymbol{Q_0}$, irrespective of the capacitance. If, on the other hand, V_S and R_S are selected in such a way that the DC load line crosses the I versus V locus in three device bias points, of which two along two separate PDR branches and one along the intermediate NDR branch, the cell admits a triplet of operating points, of which each of those (the one), corresponding to the memristor PDR operating points (to the memristor NDR operating point), is Locally Passive and Locally Stable (Locally Active yet Unstable), irrespective of C. Finally, the capacitance is found to play a decisive role on the Local Stability and Local Activity properties of the only operating point $\boldsymbol{Q_0}$, which the cell admits, when, upon a suitable choice for V_S and R_S, the DC load line intersects the I versus V locus in a NDR bias point for the memristor only. Here, $\boldsymbol{Q_0}$ is Locally Active and Asymptotically Stable, i.e. on the Edge of Chaos, if $C < \hat{C}(X)$, whereas it is Locally Active yet Unstable if $C > \hat{C}(X)$. In fact, only in the latter case, i.e. for $Q \in (Q_{NDR,L}, Q_{NDR,U})$, and $R_S > -r(Q)$, may oscillations develop across the cell. How and for which capacitance value[14] are oscillations born in the cell depends critically upon the memristor operating point $Q = X$. Yet, a *Hopf Bifurcation* is bound to occur in all circumstances for $C_{HOPF} = \hat{C}(X)$, when the operating point $\boldsymbol{Q_0}$ lies at the frontier between Stable and Unstable Local Activity domains. With reference to the capacitance sweep carried out in the case study illustrated in Fig. 6, a *Hopf Bifurcation of Subcritical type* was found to occur in the cell of Fig. 5(b) for $C_{HOPF} = \hat{C}(X = 709) =$ 9.34nF. The Hopf bifurcation is preceded by a global *Fold or Saddle-Node Limit Cycle Bifurcation*, as inferable from plot (a). For capacitance values larger than C_{HOPF} the cell phase plane admits one and only one attractor, namely a GAS limit cycle (see plot (b)). An in-depth study of this kind enables the circuit designer to make robust parameter selections to ensure the cell of Fig. 5(b) may act as an oscillator, even when, in a practical setting, certain nonidealities would perturb it away from the nominal operating conditions.

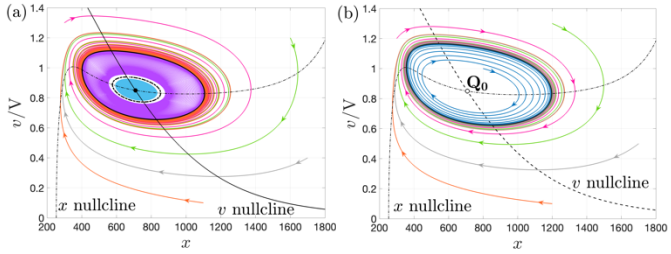

Fig. 6 (a) ((b)) Phase portrait of the ODE (6a)-(6b) for $V_S = 1.72$V, $R_S = 50\Omega$, and $C = 9.2$nF ($C = 10$nF). The memristor may admit one NDR operating point only, i.e. $Q = X = 709$, where, correspondingly, $V = 0.85$V, and $I = 17.446$mA. Increasing the capacitance value from 0F, the cell phase plane first hosts only a GAS operating point $\boldsymbol{Q_0} = (Q, V)$. When C is increased up to $C_{FOLD} = 9.021$nF, a Fold Limit Cycle Bifurcation occurs. In (a) an unstable cycle (dashed black closed orbit) is thus found to separate an outer stable cycle (solid black closed orbit) from the stable operating point $\boldsymbol{Q_0}$ (filled black circle). Increasing C further, a Hopf Subcritical Bifurcation occurs for $C_{HOPF} = \hat{C}(X) = 9.34$nF. In (b) the only attractor, appearing in the cell phase plane, is thus a limit cycle (solid black closed orbit). Here $\boldsymbol{Q_0}$ (black hollow circle) is a repellor.

The theoretical methodologies, reported in this tutorial, may be applied *mutatis mutandis* to design bio-inspired networks ([20]-[21], [37]), leveraging the local activity of other volatile memristor physical realizations, including electrothermal resistance switching memories [38], independently of their

[11] The poles of $Z_o(s)$ coincide with the eigenvalues of the ODE (6a)-(6b).

[12] As anticipated in the caption of Fig. 4, the inequality $R_S > -r(Q)$ necessarily holds true when an appropriate bias parameter pair is chosen in the circuit of Fig. 3(a) for the stabilization of a NDR operating point of the device.

[13] Without loss of generality, the voltage source in the cell of Fig. 5(b) is assumed to generate a positive DC voltage V_S. In these circumstances the DC load line crosses the DC I versus V locus of the device in the first quadrant.

[14] Studying a system, after its linearization about some operating point, offers only a partial view of its operating principles. Its global behaviour needs to be explored as well, e.g. via phase portrait analysis, to draw a complete picture of its nonlinear dynamics. Differently from the case study in Fig. 6, for $(V_S, R_S) = (1.3\text{V}, 100\Omega)$, whereby $Q = X = 389$, $V = 0.994$V, and $I = 3.060$mA, the cell of Fig. 5(b) undergoes a *Hopf Supercritical Bifurcation* for $C_{HOPF} = \hat{C}(X) = 4.083$nF [20]. Remarkably, it thus sustains all the bifurcations ([35], [36]) emerging in the Hodgkin-Huxley neuron model [27].

constitutive materials ([15], [39]), as well as ovonic threshold switches [40], and second-order diffusive memristors [41].

V. Conclusion

This tutorial has elucidated how powerful methods from Nonlinear Circuits and Systems Theory [22]-[23], including especially concepts from the Physics Principle of Local Activity [30], may be employed to support a robust design of bio-inspired circuits, which, leveraging the Negative Differential Resistance phenomena, appearing in certain solid-state volatile resistance switching memories [26], similarly as is the case for neuronal ion channels (see[15] Fig. 7), as well as the synaptic plasticity of memristors from the non-volatile class [43] may potentially boost the energy efficiency of traditional electronic systems ([19], [44]-[46]).

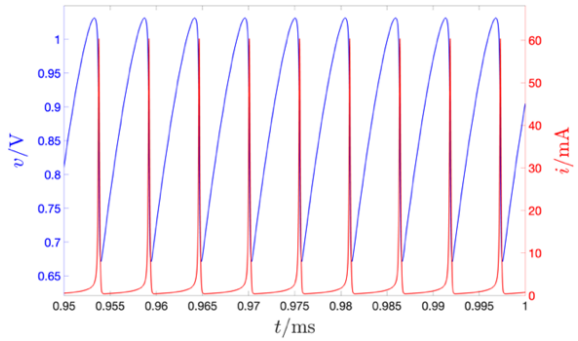

Fig. 7 Time waveform of the capacitor voltage v (blue trace) and of the memristor current i (red trace) in the relaxation oscillator from Fig. 6(b) for $V_S = 2.5\text{V}$, $R = 500\Omega$, and $C = 30\text{nF}$ and initial condition $(x_0, v_0) = (215, 0.975\text{V})$. While the capacitance voltage evolves in time as a typical integrate-and-fire relaxation oscillation, the memristor current captures the classical spiking behaviour of an action potential. This numerical example provides clear evidence for the capability of the NaMLab memristor to induce neuronal dynamics across the second-order cell [42]. Under the circuit and memristor parameter setting, employed in this simulation, the cell is found to features an oscillation frequency f of 184kHz, while consuming a net steady-state energy per cycle, indicated as $\Delta\mathcal{E}_T$, where T is the input period, of 44nJ. Note that the memristor model parameters in Table I [26] were fitted to a device sample fabricated through a suboptimal manufacturing process. Ad hoc modifications to the technology process, which produces the device physical stack, shall allow to boost the performance of the cell either for capturing biological dynamical phenomena or for computing data in compliance with some bio-inspired time- and energy-efficient paradigm in the near future.

References

[1] R. S. Williams, "What's next? [The end of Moore's law]," IEEE Computing in Science & Engineering, vol. 19, no. 2, pp. 7–13, 2017.

[2] G. E. Moore, "Cramming more components onto integrated circuits," Electronics, vol. 38, no. 8, pp. 114–117, 1965.

[15] Assuming the limit cycle on the i versus v plane to cover the NDR branch of the memristor DC locus only, the frequency of oscillation may be estimated by means of the closed-form expression $f = 1/T$, where $T = \tau_{on} + \tau_{off}$, with $\tau_{on/off} = C \cdot \tilde{R}_{off/on} \cdot \ln\left((V_{NDR,L/U} - \tilde{R}_{off/on} \cdot I_S)/(V_{NDR,U/L} - \tilde{R}_{off/on} \cdot I_S)\right)$, $I_S = V_S/R_S$, $\tilde{R}_{off/on} = R_S \parallel R_{off/on}$, and $R_{off/on} = 1/G(Q_{NDR,L/U})$. The net energy consumed by the cell over each T-long cycle at steady state may be estimated via $\Delta\mathcal{E}_T = \Delta\mathcal{E}_{\tau_{on}} + \Delta\mathcal{E}_{\tau_{off}}$, with $\Delta\mathcal{E}_{\tau_{on/off}} = I_S \cdot \left((V_S - \tilde{R}_{off/on} \cdot I_S) \cdot \tau_{on/off} - C \cdot \tilde{R}_{off/on} \cdot (V_{NDR,L/U} - \tilde{R}_{off/on} \cdot I_S) \cdot \left(1 - \exp\left(-\tau_{on/off}/(C \cdot \tilde{R}_{off/on})\right)\right)\right)$. For $Q_{NDR,L} = 351$, $Q_{NDR,U} = 1006$ $V_{NDR,L} = 0.826\text{V}$, and $V_{NDR,U} = 1.007\text{V}$, the formula for the frequency of oscillation (for the net steady-state energy absorbed by the cell per cycle) provides 229kHz (34nJ), which, given the approximations involved in its derivation, is relatively close to the simulated value in the caption of Fig. 7.

[3] D. Ielmini, and R. Waser, "Resistive Switching: From Fundamentals of Nanoionic Redox Processes to Memristive Device Applications," Wiley-VCH, 1st edition, 2016.

[4] S. Goswami, R. Pramanick, A. Patra, S.P. Rath, M. Foltin, A. Ariando, D. Thompson, T. Venkatesan, S. Goswami, and R.S. Williams, "Decision trees within a molecular memristor," Nature, vol. 597, no. 7874, pp. 51–56, 2021.

[5] C. Li, C.E. Graves, X. Sheng, D. Miller, M. Foltin, G. Pedretti, and J.P. Strachan, "Analog content-addressable memories with memristors," Nat. Commun., vol. 11, no. 1638, pp.8, 2020.

[6] D. Heim, G.L. Barbruni, and S. Carrara, "A Novel Approach in Edge Computing: In-Memory Sensing of Cancer Markers," Int. Symp. on Circuits and Systems (ISCAS), Austin, Texas, U.S., 2022

[7] P.O. Vontobel, W. Robinett, P.J. Kuekes, D.R. Stewart, J. Straznicky, and R.S. Williams, "Writing to and reading from a nano-scale crossbar memory based on memristors," Nanotechnology, vol. 20, 425204 (21pp), 2009.

[8] M. Hu, J.P. Strachan, Z. Li, E.M. Grafals, N. Davila, C. Graves, S. Lam, N. Ge, J.J. Yang, and R.S. Williams, "Dot-Product Engine for Neuromorphic Computing: Programming 1T1M Crossbar to Accelerate Matrix-Vector Multiplication," Design Automation Conference (DAC), June 5-9, Austin, Texas, U.S., 2016.

[9] B. Hoffer, V. Rana, S. Menzel, R. Waser, and S. Kvatinsky, "Experimental Demonstration of Memristor-Aided Logic (MAGIC) Using Valence Change Memory (VCM)", IEEE Transactions on Electron Devices, vol. 67, no. 8, pp. 3115-3122, 2020.

[10] A. Ascoli, R. Tetzlaff, Sung-Mo (Steve) Kang, and L.O. Chua, "Theoretical Foundations of Memristor Cellular Nonlinear Networks: A DRM2-based Method to Design Memcomputers with Dynamic Memristors," IEEE TCAS-I: Regular Papers, vol. 67, no. 8, pp. 2753-2766, 2020.

[11] M. Di Ventra, "MemComputing: Fundamentals and Applications," Oxford University Press, Oxford, 2022.

[12] Q. Xia, and J.J. Yang, "Memristive crossbar arrays for brain-inspired computing," Nature Materials, vol. 18, no. 4, pp. 309-323, 2019.

[13] M.D. Pickett, and R.S. Williams, "Sub-100 fJ and sub-nanosecond thermally driven threshold switching in niobium oxide crosspoint nanodevices," Nanotechnology, vol. 23, no. 21, pp. 215202, 2012.

[14] A. Ascoli, S. Slesazeck, H. Mähne, R. Tetzlaff, and T. Mikolajick, "Nonlinear dynamics of a locally-active memristor," IEEE Trans. Circuits and Systems (TCAS)-I: Regular Papers, vol. 62, no. 4, pp. 1165-1174, 2015.

[15] W. Yi, K.K. Tsang, S.K. Lam, X. Bai, J.A. Crowell, and E.A. Flores, "Biological plausibility and stochasticity in scalable VO2 active memristor neurons," Nat. Commun., vol. 9, no. 4661, pp. 1-10, 2018.

[16] I. Messaris, T.D. Brown, A.S. Demirkol, A. Ascoli, M.M. Al Chawa, R.S. Williams, R. Tetzlaff, and L.O. Chua, "NbO2-Mott Memristor: A Circuit-Theoretic Investigation," IEEE TCAS–I: Regular Papers, vol. 68, no. 12, pp. 4979-4992, 2021.

[17] L.O. Chua, "Hodgkin-Huxley axon is made of memristors," Int. Journal of Bifurcation and Chaos, vol. 22, no. 3, 1230011(48pp.), 2012.

[18] E.M. Izhikevich, "Dynamical Systems in Neuroscience: The Geometry of Excitability and Bursting," MIT Press, Cambridge, Massachusetts, 2007.

[19] M.D. Pickett, and R.S. Williams "Phase transitions enable computational universality in neuristor-based cellular automata," Nanotechnology, vol. 24, 384002(7pp.), 2013.

[20] A. Ascoli, A.S. Demirkol, R. Tetzlaff, and L.O. Chua, "Edge of Chaos Theory Resolves Smale Paradox," IEEE TCAS–I: Regular Papers, vol. 69, no. 3, pp. 1252–1265, 2022.

[21] A. Ascoli, A.S. Demirkol, R. Tetzlaff, and L.O. Chua, "Edge of Chaos is Sine Qua Non for Turing Instability," IEEE TCAS–I: Regular Papers, vol. 69, no. 11, pp. 4596-4609, 2022.

[22] L.O. Chua, C.A. Desoer, and E.A. Kuh, "Linear and nonlinear circuits", McGraw Hill, New York, 1987.

[23] F. Corinto, M. Forti, and L.O. Chua, "Nonlinear Circuits and Systems with Memristors: Nonlinear Dynamics and Analogue Computing via the Flux-Charge Analysis Method," Springer, 2020.

[24] K. Mainzer, and L.O. Chua, "The Local Activity Principle," Imperial College Press, 2013.

[25] J. Guckenheimer, and P. Holmes, "Nonlinear Oscillations, Dynamical Systems, and Bifurcations of Vector Fields," 1st edition, Springer-Verlag New York, Inc., New York, U.S., 1983.

[26] A. Ascoli, S.A. Demirkol, R. Tetzlaff, S. Slesazeck, T. Mikolajick, and

L.O. Chua, "On Local Activity and Edge of Chaos in a NaMLab Memristor," Frontiers in Neuroscience, vol. 15, no. 651452, 30pp., 2021.

[27] A.L. Hodgkin, and A.F. Huxley, "A quantitative description of membrane current and its application to conduction and excitation in nerve", J. Physiol., vol. 117, no. 4, pp. 500-544, 1952.

[28] A.M. Turing, "The Chemical Basis of Morphogenesis," Philosophical Transactions of the Royal Society of London, Series B, Biological Sciences, vol. 237, no. 641, pp. 37-72, 1952.

[29] S. Smale, "A Mathematical Model of Two Cells via Turing's Equation," American Mathematical Society, Lectures in Applied Mathematics, vol. 6, pp. 15-26, 1974.

[30] L.O. Chua, "Local activity is the origin of complexity," Int. Journal of Bifurcation and Chaos, vol. 15, no. 11, pp. 3435–3456, 2005.

[31] A.S. Demirkol, A. Ascoli, I. Messaris, and R. Tetzlaff, "Pattern formation dynamics in a Memristor Cellular Nonlinear Network structure with a numerically stable VO_2 memristor model," Japanese Journal of Applied Physics, vol. 61, no. 61 SM0807 (11pp.), 2022.

[32] L.O. Chua, "Resistance switching memories are memristors," Applied Physics A, vol. 102, pp. 765-783, 2011.

[33] L.O. Chua, "Five Non-Volatile Memristor Enigmas Solved," Applied Physics A, vol. 124, no. 8, 563(43pp.), 2018.

[34] A. Ascoli, S. Menzel, V. Rana, T. Kempen, I. Messaris, A.S. Demirkol, M. Schulten, A. Siemon, and R. Tetzlaff, "A Deep Study of Resistance Switching Phenomena in TaOx ReRAM cells: System-Theoretic Dynamic Route Map Analysis and Experimental Verification," Advanced Electronic Materials, vol. 8, no. 8, 2200182(31pp.), 2022.

[35] A. Ascoli, A.S. Demirkol, R. Tetzlaff, and L.O. Chua, "Edge of Chaos Theory Sheds Light into the All-to-None Phenomenon in Neurons - Part I: On the Fundamental Role of the Sodium Ion Channel," IEEE TCAS–I: Regular Papers, 2023.

[36] A. Ascoli, A.S. Demirkol, R. Tetzlaff, and L.O. Chua, "Edge of Chaos Theory Sheds Light into the All-to-None Phenomenon in Neurons - Part II: On the Necessary and Sufficient Conditions for the Observation of the Entire Life Cycle of an Action Potential," IEEE TCAS–I: Regular Papers, 2024

[37] M. Weiher, M. Herzig, R. Tetzlaff, A. Ascoli, T. Mikolajick, and S. Slesazeck, "Pattern formation with local active S-type NbOx memristors," IEEE TCAS-I: Regular Papers, vol. 66, no. 7, pp. 2627-2638, 2019

[38] T.D. Brown, S. Kumar, and R.S. Williams, "Physics-based compact modeling of electrothermal memristors: Negative differential resistance, local activity, and non-local dynamical bifurcations," Appl. Phys. Rev. 9, 011308(45pp.), 2022

[39] G.A. Gibson, S. Musunuru, J. Zhang, K. Vandenberghe, J. Lee, C.-C. Hsieh, W. Jackson, Y. Jeon, D. Henze, Z. Li, and R.S. Williams, "An accurate locally active memristor model for S-type negative differential resistance in NbOx," Appl. Phys. Lett., vol. 108, no. 2, 023505(5pp.), 2016

[40] Z. Wang, S. Joshi, S.E. Savel'ev, H. Jiang, R. Midya, P. Lin, M. Hu, N. Ge, J.P. Strachan, Z. Li, Q. Wu, M. Barnell, G.-L. Li, H.L. Xin, R.S. Williams, Q. Xia, and J.J. Yang, "Memristors with diffusive dynamics as synaptic emulators for neuromorphic computing," Nature Materials, vol. 16, no. 1, pp. 101-108, 2017

[41] S.R. Ovshinsky, "Reversible electrical switching phenomena in disordered structures," Phys. Rev. Lett., vol. 21, no. 20, pp. 1450-1453, 1968

[42] A. Ascoli, A.S. Demirkol, S. Slesazeck, T. Mikolajick, R. Tetzlaff, and L.O. Chua, "Edge of Chaos Theory Reveals the Simplest Ever Reported Hodgkin-Huxley Neuristor from NaMLab," Nat. Commun., under review.

[43] G.W. Burr, R.M. Shelby, S. Sidler, C. di Nolfo, J. Jang, I. Boybat, R.S. Shenoy, P. Narayanan, K. Virwani, E.U. Giacometti, B.N. Kurdi, and H. Hwang, "Experimental demonstration and tolerancing of a large-scale neural network (165000 synapses), using phase-change memory as the synaptic weight element," IEEE Transactions on Electron Devices, vol. 62, no. 11, pp. 3498-3507, 2015

[44] E. Corti, B. Gotsmann, K. Moselund, A.M. Ionescu, J. Robertson, S. Karg, "Scaled resistively-coupled VO2 oscillators for neuromorphic computing," Solid State Electronics, vol. 20, no. 107729 (7pp.), 2021

[45] A. Ascoli, M. Weiher, M. Herzig, S. Slesazeck, T. Mikolajick, and R. Tetzlaff, "Graph Coloring via Locally-Active Memristor Oscillatory Networks," Journal of Low Power Electronics and Applications, Special Issue on Low Power Memory/Memristor Devices and Systems, A. Serb and A. Mehonic eds., vol. 12, no. 2, 30pp., 2022

[46] Z. Wang, S. Joshi, S. Savel'ev, W. Song, R. Midya, Y. Li, M. Rao, P. Yan, S. Asapu, Y. Zhuo, H. Jiang, P. Lin, C. Li, J.H. Yoon, N.K. Upadhyay, J. Zhang, M. Hu, J.P. Strachan, M. Barnell, Q. Wu, H. Wu, R.S. Williams, Q. Xia, and J.J. Yang, "Fully memristive neural networks for pattern classification with unsupervised learning," Nature Electronics, vol. 1, no. 2, pp. 137-145, 2018

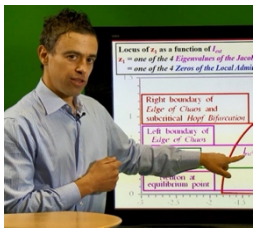

A. Ascoli (Senior Member, IEEE) received the Ph.D. Degree in Electronic Engineering from University College Dublin in 2006. Since Dec. 2023 he is with the Department of Electronics and Telecommunications, Politecnico di Torino, Turin, Italy. From Dec. 2012 to Nov. 2023, he was affiliated with the Faculty of Electrical and Computer Engineering, Technische Universität (TU) Dresden. He develops circuit- and system-theoretic methods for the analysis and design of bio-inspired memristive circuits, enabling to deepen our understanding of biological systems and/or to extend the functionalities of traditional electronic systems. He was conferred the Habilitation title as Full (Associate) Professor in Electrical Circuit Theory from the Italian Ministry of Education in 2023 (2017), and the Habilitation title as Full Professor in Nonlinear Circuit Theory from TU Dresden in 2022. He was the President of the IEEE Cellular Nanoscale Networks and Array (and Memristor Array) Computing Technical Committee from 2019 (2021) to 2021 (2023). He was honoured with the Darlington Best Paper Award from TCAS in 2023, and with Best Paper Awards from IJCTA in 2007, and from MOCAST in 2022 and 2020. He serves as Associate Editor for IEEE TCAS-I since 2023.

A.S. Demirkol received the Ph.D. degree in electronics engineering from Istanbul Technical University in 2014. He has been a Research Associate with the Chair of Fundamentals of Electrical Engineering, TU Dresden, since 2019. Previously, he was the Lead Researcher in a joint industrial project at the Chair of Fundamentals of Electrical Engineering from 2015 to 2019. His current research interests cover modeling of memristors, analysis and design of memristive systems, cellular nonlinear networks, and neuromorphic circuit design, while he has a strong research experience in distortion analysis of RF switches using Volterra series, compact device modeling, analog circuit design, active networks synthesis, nonlinear dynamics, and chaos.

R. Tetzlaff (Senior Member, IEEE) is currently the Chief Officer for technology transfer and internationalization with TU Dresden, Dresden, Germany, where he also holds a Full Professorship in fundamentals of electrical engineering. His scientific interests include problems in the theory of signals and systems, medical signal processing, stochastic processes, systems modeling, systems identification, machine learning, mem-elements, memristive systems, Volterra systems, and cellular nonlinear networks. He served as President of the IEEE Cellular Nanoscale Networks and Array Computing TC from 2005 to 2007. He was conferred the Darlington Best Paper Award from TCAS in 2023, and the Best Paper Awards from MOCAST in 2022 and 2020. In 2016 he founded the Chua Memristor Center together with T. Mikolajick, and D. Fey.

L. Chua (Life Fellow, IEEE) is widely known for his invention of the memristor. When not immersed in science, he relaxes by searching for Wagner's leitmotifs, musing over Kandinsky's chaos, and contemplating Wittgenstein's inner thoughts. His research has been recognized through 17 honorary doctorates from major universities in Europe and Japan, and holds seven U.S. patents. He was a Foreign Member of the European Academy of Sciences (Academia Europaea) in 1997 and the Hungarian Academy of Sciences in 2007. He was elected as the Confrérie des Chevaliers du Tastevin in 2000. He was conferred numerous prestigious awards, including the first Kirchhoff Award, the Guggenheim Fellow, the 2019 EDS Celebrated Member Prize—the highest recognition of the IEEE Electron Devices Society, the 2020 Julius Springer Prize in applied physics, and the Darlington Best Paper Award from TCAS in 2023.